

suggest additional photochemical mechanisms by which OCIO can contribute to O<sub>3</sub> depletion, should OCIO be adsorbed on or solvated within aerosols.

Work in progress (52) measures the sticking coefficients for OCIO on ice surfaces to obtain the OCIO content of atmospheric aerosols. Recent photochemical studies of OCIO in warm (80 to 150 K) ice matrices find quantitative conversion of OCIO to ClOO (53). Possible atmospheric consequences of OCIO in aerosols include vertical redistribution of Cl in the Antarctic vortex, release of active Cl by reaction with HCl, and heterogeneous photochemical O<sub>3</sub> depletion.

#### REFERENCES AND NOTES

- J. C. Farman, B. G. Gardiner, J. D. Shanklin, *Nature* **315**, 207 (1985).
- A. F. Tuck, T. R. Watson, E. P. Condon, J. J. Margitan, O. B. Toon, *J. Geophys. Res.* **94**, 11181 (1989).
- S. Solomon, *Nature* **347**, 347 (1990).
- World Meteorological Organization Report 20* (1990), vol. 1.
- J. G. Anderson, W. H. Brune, M. H. Proffitt, *J. Geophys. Res.* **94**, 11465 (1989).
- W. H. Brune, J. G. Anderson, K. R. Chan, *ibid.*, p. 16649.
- S. Solomon, R. W. Sanders, M. A. Carroll, A. L. Schmeltekopf, *ibid.*, p. 11393.
- C. Schiller *et al.*, *Geophys. Res. Lett.* **17**, 501 (1990).
- G. Brasseur and S. Solomon, *Aeronomy of the Middle Atmosphere* (Reidel, Dordrecht, Holland, 1986).
- S. Solomon, R. R. Garcia, F. S. Rowland, D. J. Wuebbles, *Nature* **321**, 755 (1986).
- M. A. Tolbert, *Science* **264**, 527 (1994).
- C. R. Webster *et al.*, *ibid.* **261**, 1130 (1993).
- D. R. Hanson and A. R. Ravishankara, *J. Geophys. Res.* **96**, 5081 (1991).
- M. J. Molina, T.-L. Tso, L. T. Molina, F. C.-Y. Wang, *Science* **238**, 1253 (1987).
- L. T. Molina and M. J. Molina, *J. Phys. Chem.* **91**, 433 (1987).
- S. P. Sander, R. R. Friedl, Y. L. Yung, *Science* **245**, 1095 (1989).
- M. B. McElroy, R. J. Salawitch, S. C. Wofsy, J. A. Logan, *Nature* **321**, 759 (1986).
- A. A. Turnipseed, J. W. Birks, J. G. Calvert, *J. Phys. Chem.* **95**, 4356 (1991).
- H. S. Muller and H. Willner, *Inorg. Chem.* **31**, 2527 (1992).
- V. Vaida, S. Solomon, E. C. Richard, E. Ruhl, A. Jefferson, *Nature* **342**, 405 (1989).
- K. A. Peterson and H.-J. Werner, *J. Chem. Phys.* **96**, 8948 (1992).
- S. Baer *et al.*, *ibid.* **95**, 6463 (1991).
- A. Arkel and I. Schwager, *J. Am. Chem. Soc.* **89**, 5999 (1967).
- F. J. Adrian, J. Bohandy, B. F. Kim, *J. Chem. Phys.* **85**, 2692 (1986).
- R. C. Dunn, B. N. Flanders, V. Vaida, J. D. Simon, *Spectrochim. Acta A* **48**, 1293 (1992).
- V. Vaida, K. Goudjil, J. D. Simon, B. N. Flanders, *J. Mol. Liq.* **61**, 133 (1994).
- R. C. Dunn and J. D. Simon, *J. Phys. Chem.*, in press.
- \_\_\_\_\_, *J. Am. Chem. Soc.* **114**, 4856 (1992).
- R. C. Dunn, J. Anderson, C. S. Foote, J. D. Simon, *ibid.* **115**, 5307 (1993).
- A. W. Richardson, R. W. Redding, J. C. D. Brand, *J. Mol. Spectrosc.* **29**, 93 (1973).
- K. Miyazaki, M. Tanoura, K. Tanaka, T. Tanaka, *ibid.* **116**, 435 (1986).
- C. Paillard, G. Dupre, H. AlAiteh, S. Youssefi-Stitou, *Ann. Phys. (Paris)* **14**, 641 (1989).
- J. L. Gole, *J. Phys. Chem.* **84**, 1333 (1980).
- J. A. Jafri, B. H. Lengsfeld III, C. W. Bauschlicher Jr., D. H. Phillips, *J. Chem. Phys.* **83**, 1693 (1985).
- E. C. Richard and V. Vaida, *ibid.* **94**, 153 (1991).

- \_\_\_\_\_, *ibid.*, p. 163.
- J. B. Coon, *ibid.* **14**, 665 (1946).
- S. Michielsen *et al.*, *ibid.* **74**, 3089 (1981).
- T. Baumert, J. L. Herek, A. H. Zewail, *ibid.* **99**, 4430 (1993).
- E. Ruhl, A. Jefferson, V. Vaida, *J. Phys. Chem.* **94**, 2990 (1990).
- E. Bishenden and D. J. Donaldson, *J. Chem. Phys.* **99**, 3129 (1993).
- H. F. Davis and Y. T. Lee, *J. Phys. Chem.* **96**, 5681 (1992).
- W. G. Lawrence, K. C. Clemitshaw, V. A. Apkarian, *J. Geophys. Res.* **95**, 18591 (1990).
- J. H. Glowina, J. Misewich, P. P. Sorokin, in *Supercontinuum Lasers*, R. R. Alfano, Ed. (Springer-Verlag, Berlin, 1990), pp. 1-4.
- A. J. Colussi, R. W. Redmond, J. C. Scaiano, *J. Phys. Chem.* **93**, 4783 (1989).
- A. J. Colussi, *ibid.* **94**, 8922 (1990).
- K. Johnsson, A. Engdahl, P. Ouis, B. Nelander, *J. Mol. Chem.* **293**, 137 (1993).
- \_\_\_\_\_, *J. Phys. Chem.* **96**, 5778 (1992).
- C. Reichardt, *Solvents and Solvent Effects in Organic Chemistry* (VCH, New York, 1988).
- R. L. Jones *et al.*, *J. Geophys. Res.* **94**, 11529 (1989).
- J. G. Anderson *et al.*, *ibid.*, p. 11480.
- C. J. Purcell, J. Conyers, P. Alapat, R. Parveen, *J. Phys. Chem.*, in press.
- J. T. Roberts, V. Vaida, L. A. Brown, J. D. Graham, in preparation.
- This work was supported by grants from the National Science Foundation (V.V., ATM-9222651, and J.D.S., CHE-9306485). We thank our co-workers on this project; R. C. Dunn, B. Flanders, C. Foote, J. L. Anderson, E. Richard, E. Ruhl, A. Jefferson, G. Frost, L. Brown, and S. Solomon. We also thank K. Peterson for many helpful discussions.

## RESEARCH ARTICLE

# Bent Helix Formation Between RNA Hairpins with Complementary Loops

John P. Marino, Razmic S. Gregorian Jr., Györgyi Csankovszki, Donald M. Crothers\*

The initial interaction between the ColE1 plasmid specific transcripts RNA I and RNA II, which function as antisense regulators of plasmid replication, comprises a transient complex between complementary loops found within the RNA secondary structures. Multidimensional heteronuclear magnetic resonance spectroscopy was used to characterize complexes formed between model RNA hairpins having seven nucleotide complementary loops. Seven base pairs are formed in the loop-loop helix, with continuous helical stacking of the loop residues on the 3' side of their helical stems. A sharp bend in the loop-loop helix, documented by gel electrophoresis, narrows the major groove and allows bridging of the phosphodiester backbones across the major groove in order to close the hairpin loops at their 5'-ends. The bend is further enhanced by the binding of Rom, a ColE1 encoded protein that regulates replication.

Regulation of the replication of the *Escherichia coli* plasmid ColE1 is mediated by the interaction of two plasmid encoded RNA transcripts, RNA I and RNA II, together with a plasmid encoded protein, Rom or Rop, which acts to control plasmid copy number (1). RNA I and RNA II interact initially by base-pairing between their complementary loop structures (2). Rom binds to the transiently formed intermediate complex, thus suppressing dissociation of the two RNAs and facilitating formation of a persistent hybrid duplex of the two RNAs (3), which in turn results in failure of replication initiation. The initial "kissing" (4)

interaction between complementary loops has been proposed as a structural motif of RNA interaction in other systems (5).

Studies of pairs of hairpins derived from the RNA I and RNA II transcripts demonstrated that the hairpins bind to each other solely through the interaction of their complementary loops, and that Rom specifically binds the structure formed by the interaction of these loops (6, 7). In addition, the stability of the complexes formed by these RNA hairpins varies in ways that do not correlate simply with the potential number and kind of Watson-Crick base pairs that could be formed between the complementary loops. The most striking example is the stability enhancement, 350 times greater relative to the wild type, observed for complexes formed between hairpins in which the wild-type loop sequences are inverted

J. P. Marino and R. S. Gregorian Jr. contributed equally to this work. All the authors are with the Department of Chemistry, Yale University, New Haven, CT 06511, USA.

\*To whom correspondence should be addressed.

5' to 3' (6–8). The hairpins with inverted loop sequences dissociate nearly 10,000 times more slowly than the wild-type stem loops. In addition, their association rates are 10 times slower than those observed for the wild type (6–8). For both classes it is found that full base pair complementarity among the nucleotides of the two constituent loops is required for maximal affinity (6–8).

We have characterized by multidimensional heteronuclear magnetic resonance (NMR) the loop-loop complexes formed between RNA hairpins with either complementary wild-type loop or inverted loop sequences (Fig. 1). Full base pairing between the loops was demonstrated in the inverted loop complex by imino spectroscopy; six of seven potential imino resonances were observed in the wild-type complex. The base-pair stacking patterns and ribose conformations in both complexes have also been established. While the NMR data do not provide long distance restraints requiring a bending of the helical axis of the

complex, models incorporating the required local NMR defined geometries were all strongly bent toward the major groove of the helix formed between the loops. Evidence for the bent character of the complexes was found by extending the DNA circular permutation analysis (9) to allow estimation of the extent of bending in these bimolecular RNA complexes. By analogy with the electrophoretic properties of bent DNA, we conclude that the complex is bent at the locus of the loop-loop interaction, and that the bend is further accentuated by binding of the Rom protein.

**NMR of complementary loop-loop RNA complexes.** We synthesized two pairs of RNA hairpin sequences (Fig. 1), with either the complementary wild-type loop sequences (RNA I wt and RNA II wt) or complementary inverted loop sequences (RNA I inv and RNA II inv). Uniformly  $^{15}\text{N}$ -labeled RNA hairpins were also synthesized (10). A combination of homonuclear  $^1\text{H}$  and heteronuclear  $^1\text{H}$ ,  $^{15}\text{N}$ , and  $^{31}\text{P}$  correlated NMR methods were used to define the number and type of intramolecular Watson-Crick base pairs formed, the helical stacking conformation, the ribose sugar pucker and the phosphorus chemical shifts found in the loop-loop complexes. The NMR spectra of the individual wild-type hairpins have been assigned and the structural characterization of the hairpins has confirmed the predicted secondary fold, generally a 6-bp (base pair) stem helix with 7-bp loop (11). The RNA I wild-type hairpin, however, was found to contain a distinctive, highly structured loop with additional base pairs and complete nucleotide stacking (11). This structure may account for the more rapid formation of the wild-type complex, which in turn may be the basis for evolutionary selection of that sequence.

Complex formation between hairpins could be monitored by observing the changes in the imino region of the  $^1\text{H}$  NMR spectra when two hairpins with complementary loops were mixed in the presence of  $\text{Mg}^{2+}$  counterion. The imino spectra were assigned by two-dimensional (2D)  $^1\text{H}$ - $^{15}\text{N}$  HMQC (heteronuclear multiple quantum correlation) and by 2D  $^1\text{H}$  NOESY (nuclear Overhauser exchange spectroscopy) in  $\text{H}_2\text{O}$  (12). To facilitate unambiguous assignment of the imino resonances and their NOE (nuclear Overhauser effect) correlates to a given hairpin within the complex, we mixed  $^{15}\text{N}$ -labeled hairpins with their unlabeled complements. The resonances belonging to the  $^{15}\text{N}$ -labeled hairpin could be selectively observed when  $^{15}\text{N}$ -selected or  $^{15}\text{N}$ -filtered NMR techniques were used.

Eleven resolved imino resonances were seen in an  $^1\text{H}$ - $^{15}\text{N}$  HMQC spectrum (12) of the complex formed by the wild-type loop sequences in which RNA I was  $^{15}\text{N}$ -labeled (Fig. 2A). Six of these imino resonances were assigned to the RNA I stem helix and five resulted from base-pairing in the loop-loop helix, in which the base-pair imino proton was donated by the RNA I strand. The same region of a  $^1\text{H}$ - $^{15}\text{N}$  HMQC spectrum taken with the complex formed by the inverted loop sequences, with an  $^{15}\text{N}$ -labeled RNA I hairpin, showed 12 resolvable resonances (imino resonance assignments for G15 and G11 required additional correlations found in the 2D NOESY spectrum in  $\text{H}_2\text{O}$ ) (Fig. 2B). Six of these imino resonances were assigned to the RNA I stem helix and six result from base-pairing in the loop-loop helix, in which the imino proton was donated by the RNA I strand. The 2D HMQC experiment not only served to disperse the  $^1\text{H}$  spectrum, but also allowed

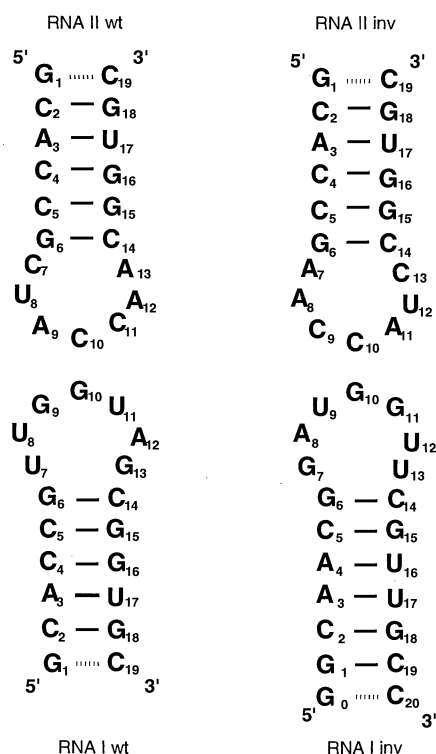


**Fig. 1.** The sequence and predicted secondary structures of the RNA I hairpin and RNA II hairpin for the wild-type (left) and inverted-loop sequences (right). The RNA I inverted loop transcript was designed and synthesized with an additional stem base-pair for stability reasons. In addition, the lower stem sequence was altered to differentiate it from the wild-type sequence in order to disfavor duplex formation between these hairpins. The numbering for the RNA I inverted loop transcript begins with zero to keep the loop numbering schemes consistent between the two sets of molecules (that is, the loop residues are labeled as positions 7 through 13 in all four stem-loops).

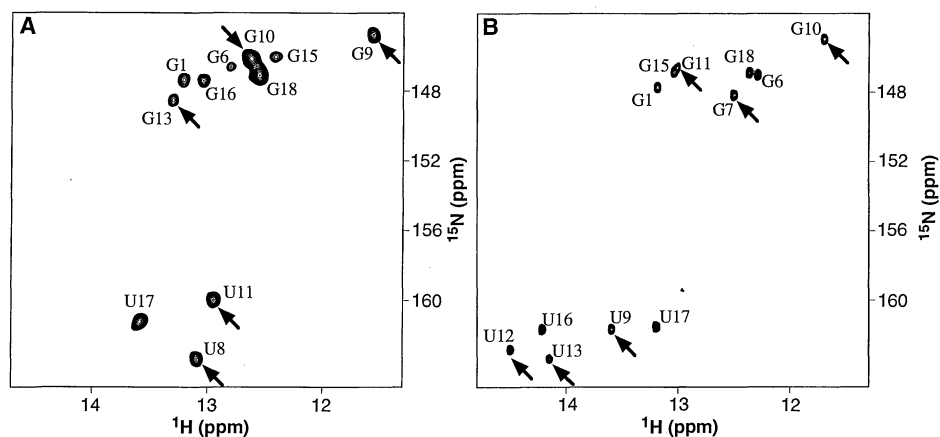


**Fig. 2.** An expansion of the imino  $^1\text{H}$ ,  $^{15}\text{N}$  resonance region of a 2D gradient enhanced  $^1\text{H}$ - $^{15}\text{N}$  HMQC experiment (12) showing imino resonance correlation for the uniformly  $^{15}\text{N}$ -labeled RNA I stem-loop complexed with an unlabeled RNA II stem-loop for the wild-type sequences (A) and the inverted loop sequences (B). The imino  $^1\text{H}$ ,  $^{15}\text{N}$  cross-peaks observed in the HMQC are assigned for each complex spectrum, with the resonances that result from the formation of the base pairs of the loop-loop helix indicated by arrows.

identification of imino protons by base type (uracil or guanine) because of their characteristic  $^{15}\text{N}$  chemical shift differences. Assignments made in this way, with further  $^{15}\text{N}$  selective experiments in  $\text{H}_2\text{O}$  on complexes formed with the wild-type loop sequences where the RNA II hairpin was uniformly  $^{15}\text{N}$ -labeled, indicated that all seven of the

potential imino resonances from the loop-loop helix were observed in the complexes formed between hairpins having inverted loop sequences. In the complex formed by the wild-type loop sequences, one of the seven potential imino proton resonances was not observed, namely that associated with the potential base pair between R1U7 and

R2A13 at one end of the loop-loop helix. Although this imino resonance was not detectable, NOE evidence for the stacking of the base pair was found in a NOESY experiment in  $\text{D}_2\text{O}$  (11, 12).

The analysis of the  $^1\text{H}$  NOESY spectrum in  $\text{H}_2\text{O}$  at  $15^\circ\text{C}$  (12) indicated that the overall topology of the wild-type and inverted loop complexes were quite similar in terms of base pair formation and stacking. Since the line widths of the wild-type complex were observed to be broader than the more stable inverted loop complex, indicative of intermediate conformational exchange, the discussion below is focused on the inverted loop complex.

The imino-imino region of a 2D  $^1\text{H}$  NOESY spectrum in  $\text{H}_2\text{O}$  (Fig. 3A) of the inverted loop complex showed sequential NOE connectivities of the two stem helices and the loop-loop helix. These connectivities established stacking of all of the base pairs in the loop-loop helix between the two stem helices and indicated that the loop residues had a continuous helical and stacked geometry on the 3' side of the respective stem helices. These experiments ruled out the alternative possibility of continuous helical stacking of the loop on the 5' side of its stem helix. The critical NOEs that connect the RNA I stem G6 imino resonance with the RNA I loop U13 imino resonance and that connect the RNA II stem G6 imino resonance with the RNA I loop G7 imino resonance are boxed.

In the complex formed with complementary inverted loops, the stacking of the base pairs could be further shown by sequential NOE correlations in  $\text{D}_2\text{O}$  at  $25^\circ\text{C}$  between the ribose H1' protons and the aromatic H6, H8 and H2 protons (Fig. 3B). The sequential anomeric aromatic NOE "walk" in the expanded plot (Fig. 3B) of the H1', H5 to aromatic H2, H6, H8 region of the  $\text{D}_2\text{O}$  NOESY of the complex formed between inverted sequence hairpins showed that the loop-loop helix is stacked between the two stem helices. The loop nucleotides of each stem loop were found to stack in a continuous helix on the 3' side of their respective stem helices, in agreement with the polarity and continuity of the loop-loop helix deduced from the imino region of the  $\text{H}_2\text{O}$  NOESY. In addition to the sequential anomeric-aromatic NOE walk that connected the helical regions, the correlation of H2 protons with H1' were also indicative of the stacked helical conformation. In the inverted loop complexes, the A·U base pairs at the first, second, and fifth positions (counting from the RNA I stem) of the loop-loop helix displayed the characteristically strong imino to H2 NOE correlation and also the H2 to H1' (intrastrand) and H1' (cross strand) NOEs found in A-form helical geometry. These NOE correlations

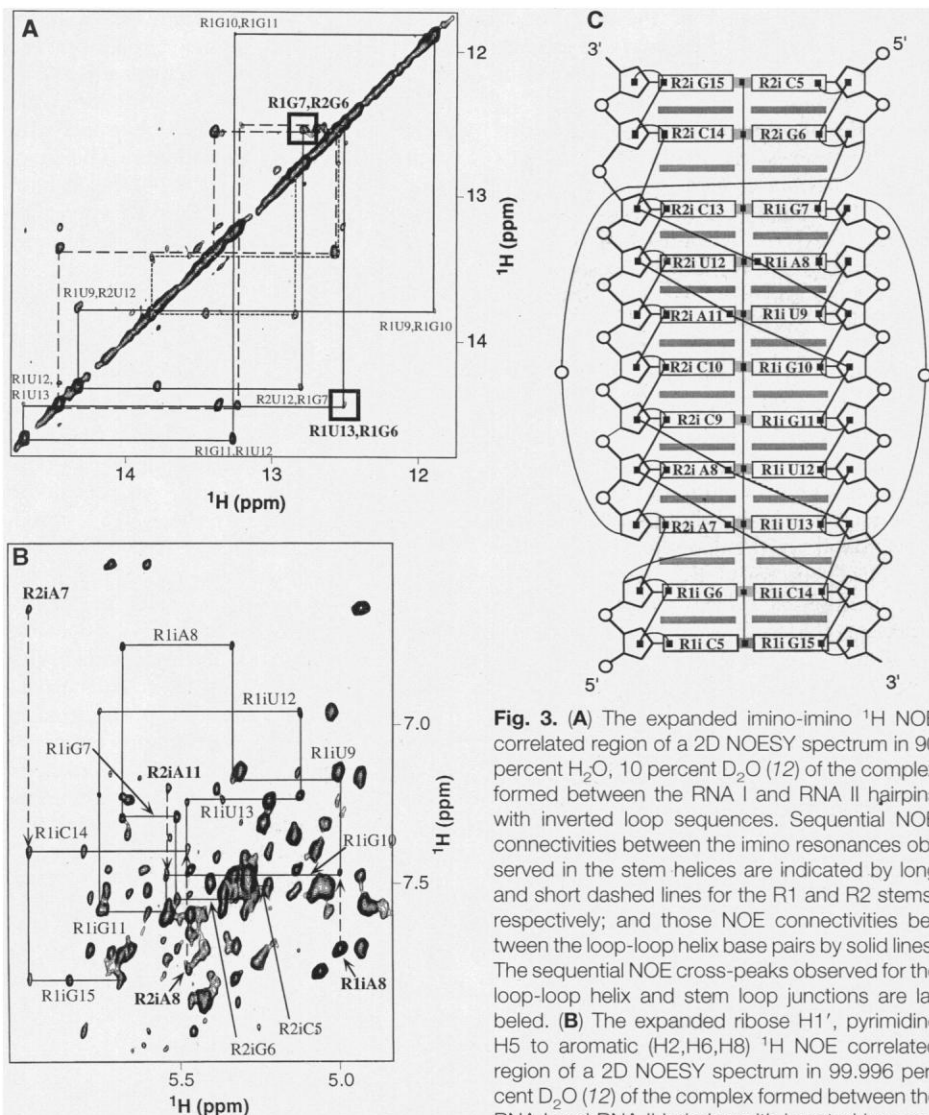


**Fig. 3.** (A) The expanded imino-imino  $^1\text{H}$  NOE correlated region of a 2D NOESY spectrum in 90 percent  $\text{H}_2\text{O}$ , 10 percent  $\text{D}_2\text{O}$  (12) of the complex formed between the RNA I and RNA II hairpins with inverted loop sequences. Sequential NOE connectivities between the imino resonances observed in the stem helices are indicated by long and short dashed lines for the R1 and R2 stems, respectively; and those NOE connectivities between the loop-loop helix base pairs by solid lines. The sequential NOE cross-peaks observed for the loop-loop helix and stem loop junctions are labeled. (B) The expanded ribose H1', pyrimidine H5 to aromatic (H2, H6, H8)  $^1\text{H}$  NOE correlated region of a 2D NOESY spectrum in 99.996 percent  $\text{D}_2\text{O}$  (12) of the complex formed between the RNA I and RNA II hairpins with inverted loop sequences.

Sequential NOEs between H8-H6 ( $n + 1$ ) and sugar H1' ( $n$ ) protons are indicated by a solid line for the RNA I and the RNA II stem-loop strands from the top two base pairs in the stems through the loop nucleotides for the pseudo-continuous helical strand from residues R2iC5 through R1iG15. The critical sequential NOEs at the stem-loop junction are those between nucleotides R1iC14 and R1iU13 ( $i$ , inverted), and also nucleotides R1iG7 and R2iG6. These connectivities are consistent with a 3' stack of the loop nucleotides on their respective stems. NOE correlations between H2 protons and H1' protons are labeled in bold, and dashed arrows show that the H1' chemical shifts are in line with the correct positions of the traced backbone NOE "walk." (C) Schematic structure of the RNA I-RNA II inverted loop complex that summarizes the NMR results. For clarity only the first two nucleotides in each stem are drawn. The residues in the remaining portion of the stems were found to display NOEs that were indicative of a standard A-form geometry. The connection between the sixth and seventh residues in the hairpins is drawn only to show strand connectivities and has no structural relevance. Base-pair hydrogen bonding is shown by wide solid lines between base-pair rectangles. Ribose H1', base H8, H6, adenine H2, and imino protons are represented by dots within pentagons, on the outside of the rectangular bases, on the inside of adenines base rectangles, or within base-base hydrogen bonds, respectively. Observed intra- and inter-nucleotide NOEs are indicated by solid lines connecting the dots. Base-pair stacking is indicated by thin, shaded boxes between the stacked base pairs.

are indicated in Fig. 3B for the pseudo-continuous helical strand formed by residues R2iC5 through R1iG15. A similar NOE walk can be made for the pseudo-continuous helical strand formed by residues R2iG15 through R1iC5. A critical cross strand NOE observed was that between the R2A7 H2 proton and the R1C14 H1' proton. This correlation provided additional evidence for the stem-loop helical stacking at that junction. Taken together, the imino NOE correlations and the anomeric-aromatic NOE correlations provided decisive evidence for the formation, coaxial stacking, and polarity of the loop-loop helix between the two hairpin stem helices. Moreover, the sequential and cross strand NOEs observed for the loop-loop helical resonances indicated that there are only minor distortions from helical geometry in the loop-loop interaction.

Analysis of the changes in chemical shift of the hairpin resonances on binding provided additional evidence that the complex interaction was a result of the stacking and pairing of nucleotides in the loops. Large chemical shift changes were observed for most loop residue resonances, while only small changes were observed for the resonances of the stem helices below the second base pair from the apical stem-loop junction. This is consistent with mutational and thermodynamic data indicating that only the first two nucleotides in from the loop-stem junction play a role in complex stability (6–8). Although the backbone geometry is not well defined for this complex, the H1',H2' region of the COSY (correlation spectroscopy) spectrum (11, 12) indicates that all ribose sugars in the complex appeared to be predominately in a C3' endo conformation (with the exception of the end residues in the stems). Furthermore, none of the phosphorus resonances are conspicuous outliers (11, 12) from what would be expected from the standard A-form chemical shift region (13).

A three-dimensional model of the complex formed with inverted complementary loops was calculated with the distance and torsional constraints derived from the NOESY and COSY experiments (14, 15). Using the protocols in X-PLOR (14), we built starting structures with a distance geometry algorithm and then refined them by a series of restrained molecular dynamics calculations (15). Although the NMR data mainly define local geometries and do not provide direct evidence for a global bending of the overall helical axis of the complex, the requirement for coaxial stacking of all seven base pairs between the stem helices was quite suggestive of a bending distortion that must occur to accomplish this overall fold. A stereoview of one of the refined

calculated models of the inverted loop-loop complex (Fig. 4A) revealed that the helical axis of the modeled complex was indeed distorted to fit the combined data and topological constraints. The model incorpo-

rated all the NMR connectivity constraints, which are shown schematically in Fig. 4C for the inverted loop hairpin complex. In repeated calculations, all the models that were generated had the essential features of

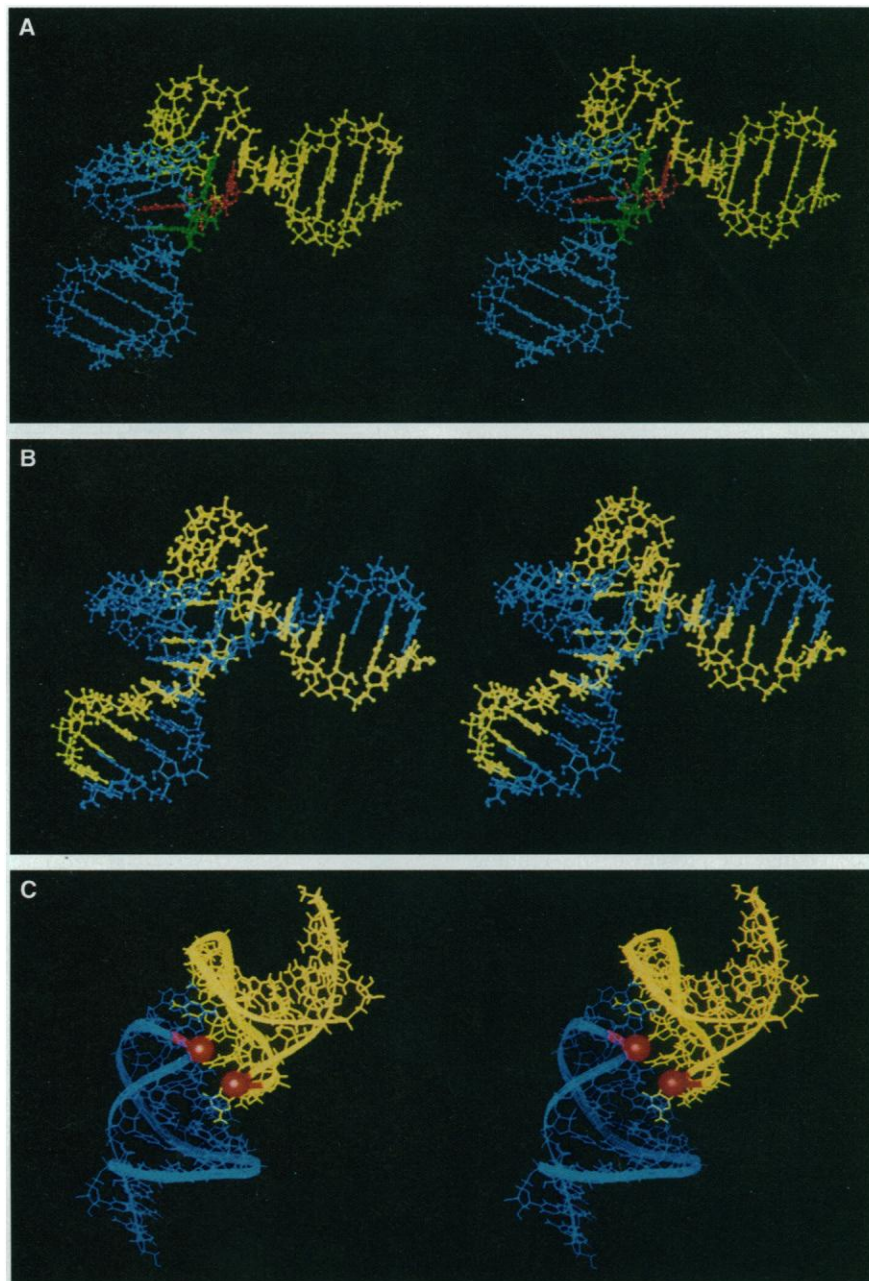


**Fig. 4.** (A) Stereo view of the three-dimensional NMR-derived model constructed for the inverted loop-loop complex. The model was generated with the distance geometry and restrained molecular dynamics protocols in X-PLOR (14, 15). The RNA I inverted hairpin is in yellow and the RNA II inverted hairpin is in blue. The model shows the base-pairing and -stacking observed in the complex and the pronounced bend that is a result of the required stacking and helical geometries. The R2iG6, R2iA7 and the R1iG6, R1iG7 dinucleotide steps are shown in green and red, respectively. (B) Stereo view of the three-dimensional NMR-derived model with the continuous helical stacking observed in the complex shown by color coding the residues that make up the two pseudo-continuous strands of the distorted helix formed by the RNA hairpins. Residues R2iG1 through R2iG6 and R1iG7 through R1iC19 are shown in yellow; residues R2iC19 through R2iA7 and R1iG6 through R1iG1 are shown in blue. (C) Stereo view of the three-dimensional model showing the compressed groove and the “bridging” phosphodiester backbones (with “bridging” phosphate atoms shown in red) that connect residues R1G6, R1G7 and R2G6, R2A7. The RNA I inverted hairpin is in yellow and the RNA II inv hairpin is in blue. Ribbons are drawn to show the trace of the phosphodiester backbone of the hairpins.

a sharply bent structure with continuous stacking of the base pairs. However, because of the limited number of constraints, the structural model is under-determined and therefore a significant variation in local geometry was observed between structures.

The calculated model suggested that coaxial stacking of the 7-bp loop-loop helix was accomplished under the constraint of closing the loop by bending strongly toward the major groove. This bend shortened the distance required for bridging across the major groove. The loop-loop helix formed a rather regular helical base stacking geometry, providing for a pseudo-continuous helical strand from one stem helix through the loop-loop helix to the other stem helix (Fig. 4B).

In the model, the backbone phosphodiester linkages between the sixth and seventh nucleotides on the 5' side of the hairpin loops (Fig. 4, A and C) were adjacent in sequence, but 7 bp away in the helical structure. Their linkage is sterically feasible because of the helical periodicity that places these phosphates directly adjacent across the narrowed major groove of the A-form helix (Fig. 4C). This geometry is a direct consequence of the 3' stacking of the loop residues on their respective stem helices. If the loop residues were 5' stacked on their stems, the 3' residues which would have to be linked to close the loop would need to be linked through a much larger distance.

**Gel electrophoretic analysis of the loop-loop complex.** Bending, a well-established DNA conformational response to sequence change or protein-ligand binding, can be characterized by gel electrophoresis methods (16), which have also been used to detect bending of RNA (17, 18). To determine the existence and extent of helical distortion present in the loop-loop complex, and the extent to which the binding of the Rom protein to the RNA complex effects further helical distortion, we used a modification of the DNA circular permutation assay (9) to measure RNA-RNA complex bending. Complexes formed between stem loops with the loop-loop interaction at the center of a pseudo-continuous helix showed anomalously slow mobility in a non-denaturing polyacrylamide gel when compared with RNA complexes of similar length with the loop-loop interaction near the end of the molecule; this is the expected result if the loop-loop interaction creates a bend in the continuous helix.

The circular permutation RNA hairpin probes, containing either the RNA I or RNA II inverted complementary loop sequences (Fig. 5A), of systematically varied lengths were made by run-off transcription with T7 RNA polymerase from DNA templates (19). In all complexes, the RNA hairpin probes were mixed so that the total

number of base pairs of RNA that can be formed is fixed at 126 for the total of the two stems, plus 7 for the loop-loop helix. Both the RNA complex and the RNA complex bound by the Rom protein (20) analyzed by this method (Fig. 5B) displayed position-dependent variations in electrophoretic mobility (21). Moreover, the position-dependent change in relative mobilities observed in the two gels indicated that the bend found for the RNA loop-loop complex was further enhanced by Rom binding.

Although the orientation of the bend could not be ascertained by this circular permutation assay, the extent of bending could be roughly estimated by a comparison of the gel mobilities of the circularly permuted complexes with the gel mobilities of similarly permuted standardized constructs of known curvature, for which we used DNA fragments of 120 bp containing 2 or 3 A-tract sequences (22). (A slightly shorter DNA sequence length was chosen in partial compensation for the smaller rise per base pair for helices of the A-form as compared

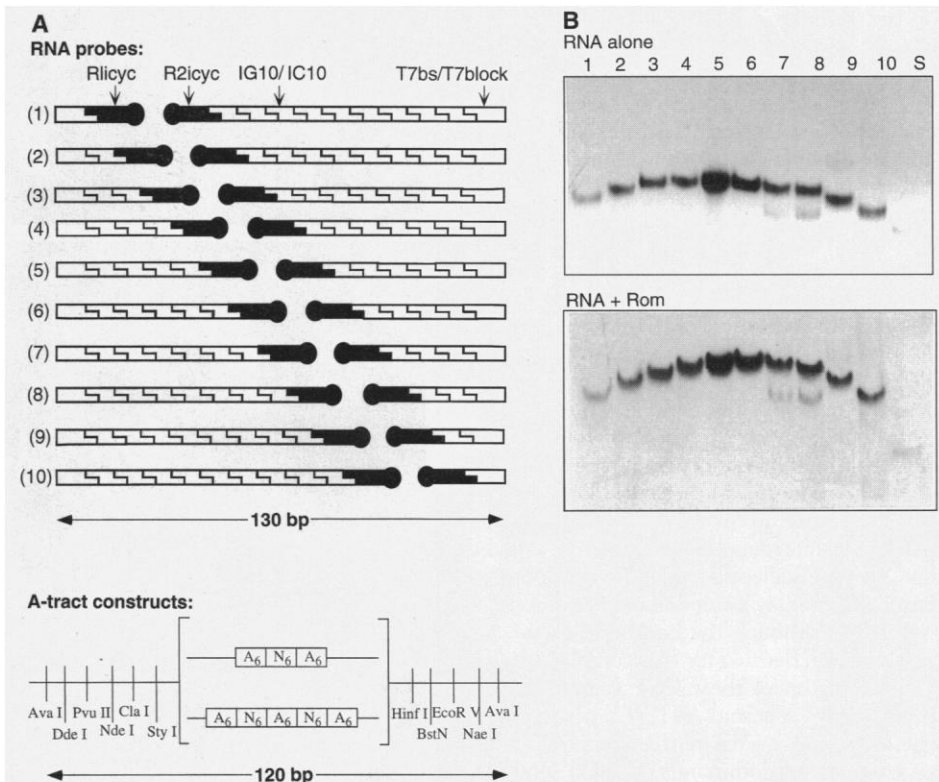


**Fig. 5.** Circular permutation analysis (9) of the distortion in the inverted stem-loop complex. **(A)** Schematics of the RNA and A-tract probes used in the circular permutation assay (8, 19). The RNAs contain the 10-bp linker sequence IG10/IC10, the T7bs-T7block duplex (which contains the T7 RNA polymerase promoter in the corresponding DNA sequence), and either the R1cyc or R2cyc hairpin sequences. The probes used to generate the two- and three-phased A-tract molecules for bend calibration were generated by restriction endonuclease cleavage at sites designed at 10-base intervals within the two flanking DNA sequences (22). **(B)** Electrophoretic mobility-shift analysis of the complexes [1 through 10 from the schematic in (A)] formed between the RNA I and RNA II hairpins with inverted-loop sequences bound to circularly permuted probes. The lane marked with an "S" was a single RNA I probe containing 128 bp plus the RI loop. Complex formation between a given pair of hairpins and mobility modulation by cyclic permutation of the loop-loop interaction site was shown with non-denaturing polyacrylamide gel electrophoresis. The same assay was performed after incubating the Rom protein with the loop-loop complexes formed between the same RNA I and RNA II hairpins bound to circularly permuted probes. **(C)** Calibration curve for estimation of the extent of bending of the loop-loop complex. The mobilities of the RNA complex, the RNA plus Rom complex, and the A-tract standards have been fit to cosine curves and are plotted as a function of position of the bend locus from the end of one of the circular permuted probes (23).

to those of the B-form.) From analysis of these results (23), we estimated a bend angle for the loop-loop complex of 45° and a bend angle for the loop-loop-Rom complex of 60°. This calibration was only approximate because it relied on comparison of molecules of different shape and potentially differing flexibility. The position of the mobility minimum indicated that the bends of the loop-loop RNA complex and the RNA-Rom complex were centered at the loop-loop interaction locus.

**Elements of RNA-RNA recognition.** Base-pairing between complementary regions and coaxial stacking of helices are commonly observed tertiary interactions in RNA structures (24). The loop-loop complex described above folds the complementary loop sequences of two independent RNA secondary elements in a pseudoknot-like (25) fashion. Complex formation is driven by the base-pairing between complementary loops and stacking of the loop-loop helix between the stem helices of the respective hairpins. As has been observed in pseudoknotted RNA structures (26), the stacking energy contributes to the binding energy of the helical interaction. In these hairpin loop complexes, differential stacking energies at the helix-helix junctions may contribute to the stability difference between wild type and inverted loop complexes.

The overall bend of the complex can be viewed as a compensatory structural change necessary for complete base-pairing and coaxial helical stacking. The energetic cost of the required backbone helical distortions is more than compensated for by the energetic gains from base-pair formation and stacking. Stable loop-loop complexes are usually formed between hairpins with loop sizes of six to eight nucleotides. As Pleij and co-workers pointed out (25), the RNA A-form major groove width to be spanned by one of the pseudoknot loops is at a minimum (10.1 Å) when the pseudoknot helix contains six to eight base pairs. This contrasts with the width of the minor groove that must be spanned by the second pseudoknot loop, which increases approximately linearly with increasing size of the pseudoknot helix. Complexes formed between hairpins with larger loop sizes or with 5'-stacking of loop residues on their respective stems, could only achieve a similar coaxially stacked structure at a much greater energetic cost to distort the RNA backbone.

Even though the complexes fold in order to minimize the distances required for loop closing across the major groove, the bend that results from complex formation (~45° to 90°) is still quite large for such a short RNA sequence. However, the large bend in DNA observed in the TBP complex gives precedent for such a structure (27); bending in that case also results from narrowing the

major groove and widening the minor groove. The sharp bend in the model structure also bears an overall resemblance to tRNA, an observation that may be of interest in view of the conjecture that tRNA might have evolved in two stages or from two separate smaller RNAs (28). Combining a hairpin having a -CCA 3' amino acid acceptor with a dumbbell shaped molecule incorporating an anticodon loop would provide an appropriate overall tRNA-like geometry in their loop-loop complex. In the ColE1 system, the bending of the loop-loop complex may play a functional role in bringing together distal regions of the larger RNA I and RNA II transcripts and thereby facilitate further folding after the initial loop-loop interactions.

**Implications for Rom recognition.** Rom is a four helix-bundle protein whose structure has been characterized both by diffraction (29) and NMR methods (30). Mutational analysis of the solvent exposed amino acids has revealed that the important residues for RNA binding are all located on helix I of the helix-loop-helix monomers and are consequently all found on a single face of the antiparallel four-helix dimer (31). Nonetheless, the key to Rom's specificity for the loop-loop structure over generic A-form RNA is not apparent in the protein structure alone. The key recognition element, however, could reside in the bent helical RNA structure created by the interaction of the two hairpins rather than in recognition of a specific nucleotide sequence. The ability of complementary loops to form the distorted helical fold seems to be the primary requirement for specific recognition. In addition, the phosphodiester residues that bridge the compressed major groove of this RNA complex provide a potentially attractive sequence-neutral recognition element for Rom binding.

The prior organization of this RNA complex into a form that favors protein binding contrasts with the Tat-TAR interaction, in which the RNA structure is reorganized upon binding peptides taken from the HIV transactivating or Tat protein to the HIV RNA sequence target TAR (32). It can be inferred that the RNA bending distortion is an important element in the protein-RNA complex structure, since Rom binding increases the bend angle beyond that seen in the RNA loop-loop complex. This observation provides a possible explanation for the preference of Rom for the loop-loop complex over normal A-form RNA, since prior bending of the RNA in the loop-loop complex should reduce the free energy required for the distortion relative to the A-form helix. This is analogous to enhanced binding affinity observed for DNA bending proteins when the DNA binding site has already been bent (33).

## REFERENCES AND NOTES

1. Y. Eguchi, T. Itoh, J. Tomizawa, *Annu. Rev. Biochem.* **60**, 631 (1991); R. W. Simons and N. Kleckner, *Annu. Rev. Genet.* **22**, 567 (1988).
2. J. Tomizawa, *J. Mol. Biol.* **212**, 683 (1990).
3. ———, *ibid.*, p. 695.
4. ———, *Cell* **38**, 861 (1984).
5. K.-Y. Chang and I. Tinoco Jr., *Proc. Natl. Acad. Sci. U.S.A.* **91**, 8705 (1994); C. Persson, E. G. Wagner, K. Nordstrom, *EMBO J.* **9**, 3767 (1990); H. Leffers, J. Kjems, L. Østergaard, N. Larsen, R. J. Garrett, *J. Mol. Biol.* **195**, 43 (1987); P. J. Cascone, T. F. Hayward, A. E. Simon, *Science* **260**, 801 (1993).
6. Y. Eguchi and J. Tomizawa, *J. Mol. Biol.* **220**, 831 (1991).
7. R. S. Gregorian Jr. and D. M. Crothers, *J. Mol. Biol.*, in press.
8. R. S. Gregorian Jr., thesis, Yale University (1994).
9. H. M. Wu and D. M. Crothers, *Nature* **308**, 509 (1984).
10. All NMR samples were synthesized by T7 run-off transcription (34) and purified by standard gel electrophoresis methods. Unlabeled samples were synthesized with commercially available NTP (nucleotide triphosphates). The <sup>15</sup>N-labeled NTPs were prepared from RNA isolated from *E. coli* grown in minimal media with <sup>15</sup>NH<sub>4</sub>Cl as the sole nitrogen source (35). NMR experiments were performed with RNA sample concentrations of 1.0 to 1.5 mM (with the exception of the <sup>15</sup>N-labeled RNA I inverted loop sample, which was 0.4 mM) in 5 mM Mg<sub>2</sub>Cl<sub>2</sub>, 50 mM NaCl, and 1 mM cacodylate, pH 6.5.
11. J. P. Marino, thesis, Yale University (1995).
12. The exchangeable imino, amino, and aromatic H2 and H5 protons for the hairpins and complexes were assigned by means of 300-ms gradient-enhanced NOESY experiments in 90 percent H<sub>2</sub>O with 10 percent D<sub>2</sub>O. The spectra were collected at 15°C with the use of a standard NOESY pulse sequence in which the last 90° pulse was replaced by a gradient-enhanced 1-1 spin echo pulse sequence (36). The 2D NOESY experiments spectra were acquired with 256 and 1024 complex points in *t*<sub>1</sub> and *t*<sub>2</sub> with 64 scans per *t*<sub>1</sub>, *t*<sub>2</sub> increment and spectral widths of 10,000 Hz in each dimension. Gradient-enhanced <sup>1</sup>H-<sup>15</sup>N HMQC (36) and <sup>15</sup>N-filtered 300-ms NOESY experiments were also collected in 90 percent H<sub>2</sub>O, 10 percent D<sub>2</sub>O at 15°C with selective off-resonance excitation accomplished with gradient-enhanced 1-1 spin echo pulses incorporated in the context of the proton pulses of the experiment (36). The HMQC spectra were acquired with 64 and 512 complex points in *t*<sub>1</sub> and *t*<sub>2</sub> with 16 scans per *t*<sub>1</sub>, *t*<sub>2</sub> increment and spectral widths of 1600 and 10,000 Hz, respectively. The <sup>15</sup>N-filtered NOESY experiments [G. Otting and K. Wüthrich, *Q. Rev. Biophys.* **23**, 39 (1990)] were acquired with 128 and 512 complex points in *t*<sub>1</sub> and *t*<sub>2</sub> with 64 scans per *t*<sub>1</sub>, *t*<sub>2</sub> increment and spectral widths of 10,000 Hz in each dimension. These experiments were collected on a GE Omega 500 spectrometer with *x*, *y*, *z* gradients applied for 1 ms during the spin echo delays in the NOESYs and during defocusing-refocusing periods of the HMQCs to eliminate transverse H<sub>2</sub>O magnetization not refocused by the selective 180° pulse. Assignment of the nonexchangeable aromatic H2, H5, H6, H8, and the H1', H2' proton resonances was made with NOESY, COSY, DQF-COSY, and <sup>1</sup>H-<sup>15</sup>N HMBIC experiments collected in 99.996 percent D<sub>2</sub>O performed on either a GE Omega 500 or a Bruker AM500 spectrometer at 25°C. The 2D NOESY and COSY experiments were collected with standard pulse sequences [K. Wüthrich, *NMR of Proteins and Nucleic Acids* (Wiley, New York, 1986)]. For both experiments, 256 and 1024 complex points in *t*<sub>1</sub> and *t*<sub>2</sub> were acquired with 32 scans per *t*<sub>1</sub>, *t*<sub>2</sub> increment. The NOE mixing time (*t*<sub>m</sub>) was 300 ms. The <sup>1</sup>H-<sup>15</sup>N refocused HMBIC experiment was collected with 128 and 512 complex points in *t*<sub>1</sub> and *t*<sub>2</sub> with 64 scans per *t*<sub>1</sub>, *t*<sub>2</sub> increment. Sequential NOEs from anomeric ribose H1' protons to aromatic H6-H8 protons were established with the NOESY; pyrimidine base H5, H6 and ribose H1', H2' correlated cross-peaks were identified by the COSY, and aromatic resonances (H2, H5, H8) were identified by correlation to specific base nitrogens in

- the refocused HMBC. One-dimensional phosphorus spectra were taken to determine the chemical shift ranges for these resonances in the complexes; however, phosphorus correlated experiments were not used for assignment of the complexes. All spectra were processed on an Indigo workstation (Silicon Graphics) with Felix software (Biosym Technologies, San Diego, CA).
13. P. Legault and A. Pardi, *J. Magn. Reson. Ser. B* **103**, 82 (1994).
  14. A. Brünger, *X-PLOR, A System for X-ray Crystallography and NMR* (Yale Univ. Press, New Haven, CT, 1992).
  15. Models for the loop-loop complex were calculated by means of distance geometry and molecular dynamics routines in X-PLOR (14) and displayed with Insight II (Biosym Technologies). Restraints used in the X-PLOR calculation included exchangeable NOEs from imino to imino and from imino to amino and H2 (adenine) resonances that were taken from the H<sub>2</sub>O NOESY experiments (observed exchangeable proton NOEs were characterized as 3.5 ± 1.0 Å) and NOEs from the H1' to aromatic H6, H8, and H2 resonances taken from the D<sub>2</sub>O NOESY experiment [nonexchangeable proton NOEs were characterized as strong (2.4 ± 0.5 Å), medium (3.0 ± 1.0 Å), and weak (4.5 ± 1.5 Å)]. Some H2' to aromatic H6-H8 NOEs were identified, but this region of the spectrum displayed much greater chemical shift overlap and so was interpreted in only a limited way. In the lower stem regions, the first four base pairs of both the RNA I and RNA II hairpins, the bond angles, and distance restraints used in the calculations were taken from W. Saenger [*Principles of Nucleic Acid Structure* (Springer-Verlag, New York, 1988)] for a standard A-form helix. Experimental NOE restraints in this region included 91 inter-residue and 36 intra-residue constraints. In the upper two base pairs of each helix and in the loops there were a total of 64 inter-residue and 44 intra-residue constraints. Pseudo-NOEs were used to define the hydrogen bonding network for all base pairs in the complex, with a total of six proton-heavy atom constraints for each GC pair and four for each AU pair. To define the ribose sugar pucker, the absence of ribose H1', H2' cross-peaks in the COSY experiment for all but the terminal bases in the stems was used to constrain the sugar puckers as C3'-endo (in a C3'-endo conformation, <sup>3</sup>J(H1', H2') < 2 Hz). All bases in the loop-loop complex were required to be in the *anti* conformation and a small energy term (50 kcal/Å<sup>2</sup>) was included to limit the freedom of base pairs to depart from planarity. All backbone angles were loosely constrained (±15° in the lower four base-pair residues of the hairpin stems and ±30° for the top two stem base-pair and the loop residues) to lie in the expected A-form geometry in the first round of distance geometry embedding and simulated annealing, after which those structures with the correct loop-loop topology (that is, structures without catenated loops) were further refined with the backbone angular restraints completely relaxed for the top two stem base-pair and "loop" residues. The loop-loop structures were refined by several rounds of simulated annealing by first fitting them to a template coordinate set to correct local geometry. Each structure was then heated to 2000°K and the NMR restraints were applied. The bond, angle, and improper energy terms were simultaneously included. After equilibrating the molecule for 6 ps at high temperature, a repulsive Van der Waals term was turned on, and each structure was slowly cooled to 100°K. No electrostatic term was included in the calculation.
  16. Reviewed by D. M. Crothers, M. R. Gartenberg, T. E. Shrader, *Methods Enzymol.* **208**, 118 (1991); D. M. Crothers and J. Drak, *ibid.* **212B**, 46 (1992).
  17. A. Bhattacharyya, A. I. Murchie, D. M. Lilley, *Nature* **343**, 484 (1990).
  18. R. S. Tang and D. E. Draper, *Biochemistry* **29**, 5232 (1990).
  19. The DNA templates were built from the following constituent pieces (8): (i) T7b, which contains the T7 promoter bottom strand; (ii) T7block, which anneals to T7b and facilitates its attachment to multimers; (iii) IG-10, IC-10, and their tandem repeats IG-20 and IC-20, which are linkers of 10 or 20 nucleotides, respectively, in length with 2-nt overhangs; and (iv) R1cyc and R2cyc templates encoding the hairpin loop sequences. DNAs were synthesized by standard phosphoramidite chemistry on an Applied Biosystems 380B DNA synthesizer, and phosphorylated at their 5' ends with T4 DNA polynucleotide kinase (New England Biolabs) in the commercial buffer, supplemented with additional ATP to a final concentration of 10 mM, for 60 minutes at 37°C. T7b was first labeled at the 5' end by incubation with [ $\gamma$ -<sup>32</sup>P]ATP (New England Nuclear, 6000 Ci mmol<sup>-1</sup>) and T4 DNA polynucleotide kinase for 30 minutes followed by an additional incubation with unlabeled ATP (added to a final concentration of 10 mM) for 30 minutes. IG-10 and IC-10, IG-20 and IC-20, and T7b and T7block were then mixed at equimolar concentration, heated to 90°C and slowly cooled to hybridize the complementary DNA strands. DNA template components were then ligated in two stages with T4 DNA ligase in the commercial buffer supplemented with ATP to a 2.5 mM final concentration. In the first ligation, the T7b-T7block hybrid was mixed with either the IG-IC-10 or IG-IC-20 hybrids, or with a mixture of both at a 1:10 molar ratio. The final mixture was ligated (overnight at 15°C), precipitated with ethanol, and fractionated on an 8 percent nondenaturing polyacrylamide gel in a buffer of 89 mM tris, 89 mM boric acid, pH 8.3, and 0.1 mM EDTA. The observed ligation ladder consists of the T7b-T7block duplex ligated onto increasing numbers of the IG-IC-10 or -20 monomers. These multimers were excised from the gel, eluted at 37°C overnight, and precipitated with ethanol. Each of the excised DNA multimers was then "capped" with one of the "cyc" end-pieces to make a hairpin template. The cyclic end-piece was added in excess (about four times more) to linear duplex DNA, and the pieces were ligated as above. Reactions were quenched at 65°C. The ethanol-precipitated products were used for transcription by T7 RNA polymerase without further purification [ $\alpha$ -<sup>32</sup>P]UTP (10  $\mu$ Ci) was added to transcription mixtures to produce body-labeled RNA hairpins. Reactions were generally incubated overnight (8 to 12 hours) at 37°C and purified by standard methods on either 6 percent (longer RNAs) or 12 percent (shorter RNAs) denaturing polyacrylamide gels.
  20. Rom protein was purified as described [R. M. Lacatena, D. W. Banner, G. Cesareni, in *Mechanisms of DNA Replication and Recombination*, N. Cozarelli, Ed. (Liss, New York, 1983), pp. 327-336] as optimized in our laboratory from *E. coli* cells obtained from B. Polisky [M. Muesing, C. D. Carpenter, W. H. Klein, B. Polisky, *Gene* **31**, 155 (1984)].
  21. For each complex, separate RNAs were individually placed in 5 mM MgCl<sub>2</sub>, heated to 90°C, and cooled immediately on ice. The R1 and R2 for each reaction were then mixed on ice, incubated at 15°C for 20 minutes, and then transferred to 15 percent polyacrylamide gels (75:1, acrylamide:bis-acrylamide, 0.75 mm thick) and separated in a Hoefer constant temperature gel apparatus, at 300 V (<5 W per gel) until the xylene cyanol was at the bottom third of the gel (14 hours). The running buffer was 89 mM tris, 89 mM boric acid, pH 8.3, and 5 mM MgCl<sub>2</sub>. The bands were visualized by autoradiography.
  22. The reference DNA molecules were constructed from three separate DNA duplexes and contained either an A<sub>6</sub>-N<sub>4</sub>-A<sub>6</sub> or an A<sub>6</sub>-N<sub>5</sub>-A<sub>6</sub>-N<sub>4</sub>-A<sub>6</sub> sequence (9). Molecules with two- or three-phased A<sub>6</sub> tracts were constructed from their three constituent parts by exhaustive ligation of the components that had been synthesized, purified, and phosphorylated as above (19). Reference DNA molecules were subjected to electrophoresis under identical conditions to the loop-loop complexes (21). All reference molecules were heated to 55°C, cooled on ice, and transferred to the gels. The two- and three-phased A<sub>6</sub> tracts bend the DNA by 36° and 54°, respectively, which nearly brackets the range of mobility modulation observed from the loop-loop complexes.
  23. Gel autoradiographs were analyzed for mobility of the individual bands for each complex or A-tract standard by measuring the distance from the bottom of the wells to the middle of the band. The data were fit to a cosine curve to evaluate the projected mobility of the complex when the bend center was at the end of the DNA molecule. From this number ( $\mu$ ), the relative mobility ( $\mu_{rel}$ ) of each bend position was calculated. Comparison of the relative mobilities of the loop-loop complexes with those of the A-tract bends of known magnitude allowed estimation of the bend angle of the complex, if we assume that there is a quadratic dependence of the position-dependent anomaly on curvature (16).
  24. M. Chastain and I. Tinoco Jr., *Prog. Nucleic Acid Res. Mol. Biol.* **41**, 131 (1991); J. R. Wyatt and I. Tinoco, in *The RNA World* (Cold Spring Harbor Laboratory Press, Plainville, NY, 1993), pp. 465-497.
  25. C. W. A. Pleij, K. Rietveld, L. Bosch, *Nucleic Acids Res.* **13**, 1717 (1985).
  26. J. R. Wyatt, J. D. Puglisi, I. Tinoco Jr., *J. Mol. Biol.* **214**, 455 (1990); J. D. Puglisi, J. R. Wyatt, I. Tinoco Jr., *Acc. Chem. Res.* **24**, 152 (1991).
  27. Y. Kim, J. H. Geiger, S. Hahn, P. Sigler, *Nature* **356**, 512 (1993); J. L. Kim, D. B. Nikolov, S. K. Burley, *Nature* **356**, 520 (1993).
  28. N. Maizels and A. Weiner, *Proc. Natl. Acad. Sci. U.S.A.* **91**, 6729 (1994); P. Schimmel and B. Henderson, *ibid.*, p. 11283.
  29. D. W. Banner, M. Kokkinidis, D. Tsernoglou, *J. Mol. Biol.* **196**, 657 (1987).
  30. W. Eberle, W. Klaus, G. Cesareni, C. Sander, P. Rosch, *Biochemistry* **29**, 7402 (1990); W. Eberle, A. Pastore, C. Sander, P. Rosch, *J. Biomol. NMR* **1**, 71 (1991).
  31. L. Castagnoli et al., *EMBO J.* **8**, 621 (1989).
  32. J. D. Puglisi, R. Tan, B. J. Caman, A. D. Frankel, J. R. Williamson, *Science* **257**, 76 (1992); J. D. Puglisi, L. Chen, A. D. Frankel, J. R. Williamson, *Proc. Natl. Acad. Sci. U.S.A.* **90**, 3680 (1993).
  33. J. D. Kahn and D. M. Crothers, *Proc. Natl. Acad. Sci. U.S.A.* **89**, 6343 (1992).
  34. J. F. Milligan, D. R. Groebe, G. W. Witherell, O. C. Uhlenbeck, *Nucleic Acids Res.* **15**, 8783 (1987); J. F. Milligan, O. C. Uhlenbeck, *Methods Enzymol.* **180**, 51 (1989).
  35. R. T. Batey, M. Inada, E. Kujawinski, J. D. Puglisi, J. R. Williamson, *Nucleic Acids Res.* **20**, 4515 (1992); E. P. Nikonowicz et al., *ibid.*, p. 4507.
  36. V. Sklenar and A. Bax, *J. Magn. Reson.* **74**, 469 (1987); A. A. Szewczak, G. W. Kellogg, P. B. Moore, *FEBS Lett.* **327**, 261 (1993).
  37. We thank G. Sun for assistance with oligonucleotide synthesis; B. Polisky (Indiana University) for providing *E. coli* cells from which Rom protein was purified; and J. H. Prestegard for advice and suggestions (to J.P.M.) on the NMR experiments. Supported by the National Institutes of Health (NIH) (GM 21966) (D.M.C.), an NIH Training Grant in Biophysics (J.P.M.), and a Howard Hughes Medical Institute Predoctoral Fellowship (R.S.G.).

7 November 1994; accepted 3 April 1995